CERN SUMMER STUDENT PROGRAM 2019

WORK PROJECT REPORT

EP-AID-DT

Yields of Proton, Kaon, and Pion Production in p-Pb Collisions at $\sqrt{s_{\mathrm{NN}}}$ = 8.16 TeV

Name
Wun Kwan YAM

Supervisors
Giacomo VOLPE
Antonello DI MAURO

9 August 2019
Geneva, Switzerland

Yields of Proton, Kaon, and Pion Production in p-Pb Collisions at $\sqrt{s_{\mathrm{NN}}} = 8.16$ TeV

Wun Kwan Yam
Department of Physics, The Hong Kong University of Science and Technology, Clear Water Bay, Hong Kong, China
(Dated: August 9, 2019)

The ALICE experiment at CERN is designed to study the properties of quark-gluon plasma, a state of matter formed under extreme conditions of temperature and energy density. These conditions are thought to be similar to those just after the Big Bang, allowing scientists to probe the beginning of the universe. In the LHC, quark-gluon plasma is formed and examined through pp, p-Pb, and Pb-Pb collisions. In particular, p-Pb collisions are used to test initial state "cold nuclear matter" effects. The High Momentum Particle Identification Detector (HMPID) is one of the 19 subdetectors in ALICE and is designed to identify charged particles by exploiting the Cherenkov effect. It is able to identify with 3σ separation π/K up to $p_T = 3$ GeV/s and K/p up to $p_T = 5$ GeV/c. In this report, p-Pb data collected in 2016 during LHC Run 2 is studied. First, the HMPID detector performance is characterized by analyzing its charge measurements. Then, the number of particles identified by the HMPID is calculated by statistical unfolding of the Cherenkov angle. Finally, corrections are applied on the detector data to obtain the total particle yield of this p-Pb sample. It is observed that the particle yield has a strong p_T dependence. In the next step, the results from this study can be combined with analysis from other ALICE detectors to complete the p_T spectrum up to 20 GeV/c, and be compared with the pp and Pb-Pb collision modes to further study quark-gluon plasma.

I. INTRODUCTION

Under extreme conditions of temperature and density, hadronic matter "melts" into a plasma of free quarks and gluons called the quark-gluon plasma (QGP) [1]. These conditions are thought to be similar to just after the Big Bang [2]. Thus, by studying QGP, it becomes possible to probe the beginning of the universe. The properties of QGP would also provide information about the theory of quantum chromodynamics (QCD), answering questions about the phenomenon of confinement and the problem of chiral symmetry restoration [3]. To create the QGP state in experiment, heavy ions are collided at ultra-relativistic energies. Long-lived particles produced inside this hot volume, namely pions, kaons, and protons, can reach the surrounding detectors and be used to study properties of QGP.

A. The ALICE Experiment

A Large Ion Collider Experiment (ALICE) [4] is an experiment hosted at the European Organization for Nuclear Research (CERN). It uses the Large Hadron Collider (LHC) particle accelerator, which consists of a 27-kilometer long ring of superconducting magnets and numerous accelerting structures. The ALICE experiment specializes in characterizing the physical properties of QGP. Every year, dedicated periods of heavy ion collisions at the LHC are used to produce and study QGP. An image of the ALICE detector is depicted in Figure 1.

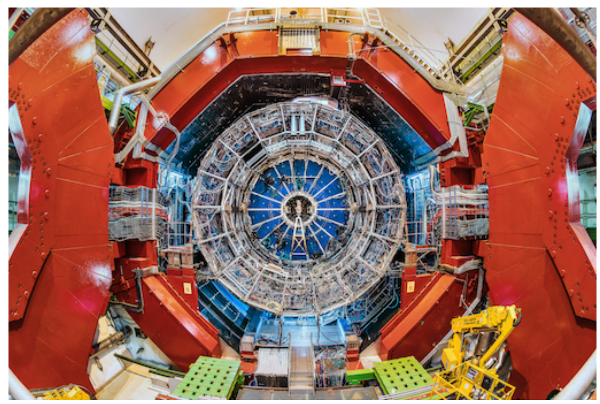

FIG. 1. Frontal view of the ALICE detector during its upgrade in Long Shutdown 2.

Three types of collisions are analyzed at the ALICE experiment, namely proton-proton (pp) collisions, proton-nucleus (pA) collisions, and nucleus-nucleus (AA) collisions. Proton-proton collisions are used as a high energy QCD reference. Proton-nucleus collisions can test initial state "cold nuclear matter" effects. Nucleus-nucleus collisions are supposed to produce the QGP state. By comparing all three types of collisions, the effects of nuclear structure and QGP can be distinguished. Lead ions are used to perform the nucleus collisions at LHC because it contains many nucleons, is stable, spherical in shape, and easily available.

The ALICE detector [4] contains 19 subdetectors that use various methods to measure the particles produced in collisions. In general, these detectors trigger data acquisition, track particle trajectories, and identify particle species [2]. It is of interest to identify particles over a large momentum range in order to study the properties of QGP. As a consequence, different detection techniques are utilized to cover different momentum ranges. Additionally, the large nucleon number in heavy ion collisions also produces high multiplicity events, which further complicates measurement.

The data analyzed in this report comes mainly from

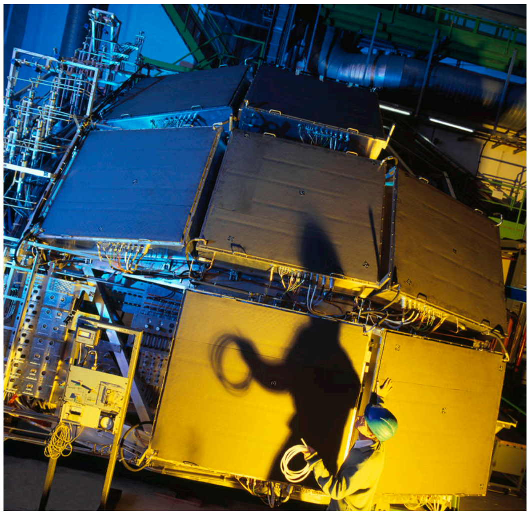

FIG. 2. Picture of the HMPID detector before its final installation inside the ALICE magnet in 2006.

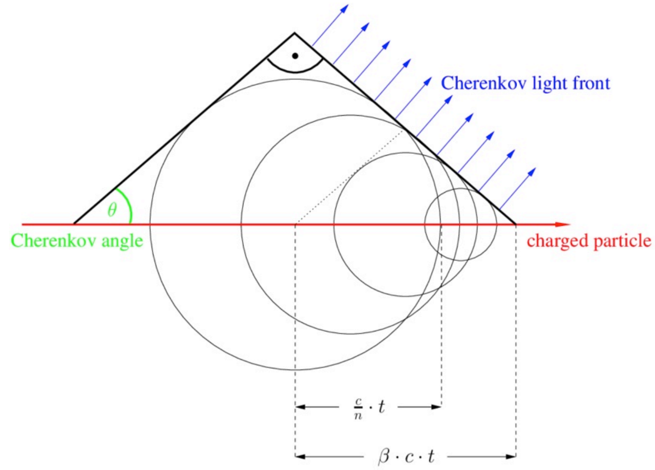

FIG. 3. Illustration of the Cherenkov effect. The Cherenkov angle θ_{Ch} is uniquely determined by the velocity β of the particle and the refractive index n of the medium.

the High Momentum Particle Identification Detector. Some relevant subdetectors for this analysis are the Inner Tracking System (ITS), the Time Projection Chamber (TPC), the Transition Radiation Detector (TRD), the V0 detector, the T0 detector, the Time of Flight (TOF) detector, the Electromagnetic Calorimeter (EMCal), and the Di-jet Calorimeter (DCal) [4]. The ITS is composed of several layers of silicon detectors and used to reconstruct the primary and secondary vertices, track particle trajectories, and identify charged particles with a low p_T cutoff. The TPC is a large cylindrical volume filled with gas, which measures particle energy loss and provides three dimensional information of particle trajectory. The TRD contains layers of materials with different dielectric constants and uses the emission of transition radiation to identify electrons and positrons. The V0 detector measures collision multiplicity and estimates centrality by summing the energy deposited on its two disks. The T0 detector serves as a start, trigger, and luminosity detector during collisions. The TOF identifies charged particles in the intermediate momentum range by making time measurements of particle trajectories. The EMCal is a lead-scintillator sampling calorimeter that measures the energy of particles, in particular photons and electrons. The DCal is a calorimeter placed opposite of the EMCal to allow the measurement of back-to-back jets and to make hadron-jet and jet-jet correlation measurements. The capabilities of these subdetectors are combined to measure particles, to identify them, and to understand the mechanisms of particle collisions in ALICE.

B. High Momentum Particle Identification Detector

The High Momentum Particle Identification Detector (HMPID) [5], shown in Figure 2, is a subdetector in ALICE used to identify charged particles, namely pions, kaons, and protons. It covers 5% of the central barrel geometrical acceptance and can identify with 3σ separation pions and kaons up to $p_T = 3$ GeV/c, and kaons and protons up to $p_T = 5$ GeV/c [6]. This extends the particle identification capabilities of ALICE beyond the energy loss measurements in the ITS and the TPC, and time measurements in the TOF detector. The momentum range above HMPID measurements is covered by TPC "relativistic rise" measurements.

HMPID consists of seven modules of proximity focusing Ring Imaging Cherenkov (RICH) chambers, which identify particles based on the Cherenkov effect [7]. When a charged particle passes through a dielectric medium with speed greater than the speed of light in that medium, photons are produced in a shock wave. The theoretical interpretation proposes that atoms in the medium become polarized along the charged particle track [8]. As the polarized atoms relax back to equilibrium, they will emit short electromagnetic pulses. In the subluminal case, these wavelets interfere destructively since the polarization field is symmetric. However, if the particle velocity exceeds the local phase velocity of light, a coherent wavefront is produced. As illustrated in Figure 3, there is a unique angle with respect to the particle track at which the wavefront is formed. This is Cherenkov radiation, and its angle θ_{Ch} is dependent on the particle velocity β by

$$\cos(\theta_{\mathrm{Ch}}) = \frac{1}{n\beta}, \tag{1}$$

where n is the refractive index of the medium. Since $|\cos(\theta_{\mathrm{Ch}})| \leq 1$, there exists a velocity threshold below which Cherenkov radiation is not produced. In order to exploit the Cherenkov effect for particle identification, HMPID measures the positions of incident charged particles and the cones of Cherenkov photons emitted.

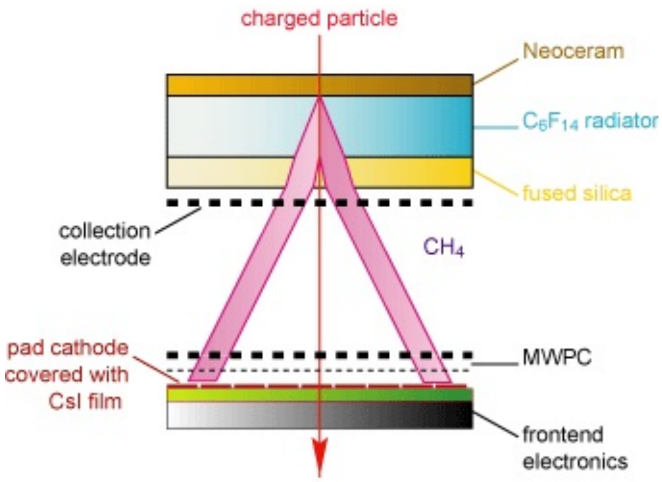

FIG. 4. Side view of RICH counters in the HMPID. A charged particle enters the chamber and produces Cherenkov photons in the C_6F_{14} radiator. The photons travel through the CH_4 proximity gap to reach the pad cathodes coated with CsI film. Electrons are produced by the photoelectric effect and their charge is measured by the MWPC.

Figure 4 shows the components of each RICH counter. Cherenkov radiation is produced when a highly energetic charged particle passes through the 15 mm thick liquid perfluorohexane (C_6F_{14}) radiator, which has $n = 1.29$. Cherenkov photons are emitted in a cone around the particle trajectory, with an opening angle θ_{Ch} dependent on its velocity β. The photons travel through the 80 mm methane (CH_4) proximity gap to reach the cathode pads coated with 300 nm cesium iodide (CsI) film. Electrons are then emitted from the CsI by the photoelectric effect, and their charge is measured by the multi-wire proportional chamber (MWPC). As a result, the detector produces images of the Cherenkov radiation in the form of rings [5]. Position of the primary charged particle is also determined by measuring its cluster charge at the MWPC. The Cherenkov angle θ_{Ch} can be deduced from the ring radius, and the particle speed β can be calculated with Equation 1. Combining the momentum and charge information measured in the tracking detectors (ITS and TPC) with the speed measured by the HMPID detector, one can deduce the particle mass and identify it. The relationship between mass and Cherenkov angle is thus

$$m = \frac{p}{c\beta\gamma} = \frac{p}{c}\sqrt{n^2\cos^2(\theta_{\text{Ch}}) - 1}. \tag{2}$$

Efficiency and contamination are features that characterize the performance of a particle identification detector [8]. Inefficiency occurs when a particle of the correct type is classified as a wrong one. Efficiency $\varepsilon_{A\to A}$ in identifying particles of type A is given by

$$\varepsilon_{A\to A} = \frac{N_{A\text{-identified}}}{N_{A\text{-total}}}, \tag{3}$$

where $N_{A\text{-identified}}$ is the number of correctly identified particles and $N_{A\text{-total}}$ is the total number of type A particles. Contamination occurs when a particle of the wrong type is classified as a correct one. Contamination $\varepsilon_{B\to A}$ in identifying particles of type A is given by

$$\varepsilon_{B\to A} = \sum_{B,B\neq A} \frac{N^B_{A\text{-identified}}}{N_{A\text{-total}}}. \tag{4}$$

where $N^B_{A\text{-identified}}$ is the number of incorrectly identified particles and $N_{A\text{-total}}$ is the total number of type A particles. When increasing particle identification efficiency, the amount of contamination will also rise. Thus, it is important to characterize "separation power" in particle identification [8]. Take S_A and S_B as the mean values of a certain quantity measured for particles of type A and B, respectively, and σ_{AB} as the mean standard deviation of the measured distributions. The separation power n_σ is defined as

$$n_\sigma = \frac{S_A - S_B}{\sigma_{AB}}. \tag{5}$$

Assuming that the measured quantities follow the Gaussian distribution, a 3σ separation ($n_\sigma = 3$) enables particle contamination to be less than 10%. When the measured populations are different, the contamination will also skew depending on the relative population sizes.

II. DATA SAMPLE AND ANALYSIS

The results in this report are obtained using data collected with the ALICE detector for proton-lead (p-Pb) collisions at $\sqrt{s_{\text{NN}}} = 8.16$ TeV in 2016 during LHC Run 2 (internally serialized as LHC16r). Because of the LHC's 2-in-1 magnet design, the energy of the proton and lead-ion beams cannot be adjusted independently and is set at 4 TeV per Z [9]. This gives different proton and lead-ion energies due to the different Z/A of the colliding protons and lead ions. Consequently, the nucleon-nucleon center-of-mass system is moving in the laboratory frame with a rapidity of $y_{\text{NN}} = -0.465$ in the direction of the proton beam. In this report, y_{lab} denotes rapidity in the laboratory reference frame and y denotes rapidity in the center-of-mass reference frame where the lead beam is assigned positive rapidity.

A. Performance characterization

The RICH chambers in HMPID measure the charges of incident minimum ionizing particles (MIP) and their emitted Cherenkov photons. This information is used to identify the MIP through the procedures in Section I B. In order to validate the results, it is thereby important to characterize the charge measurements for each RICH chamber.

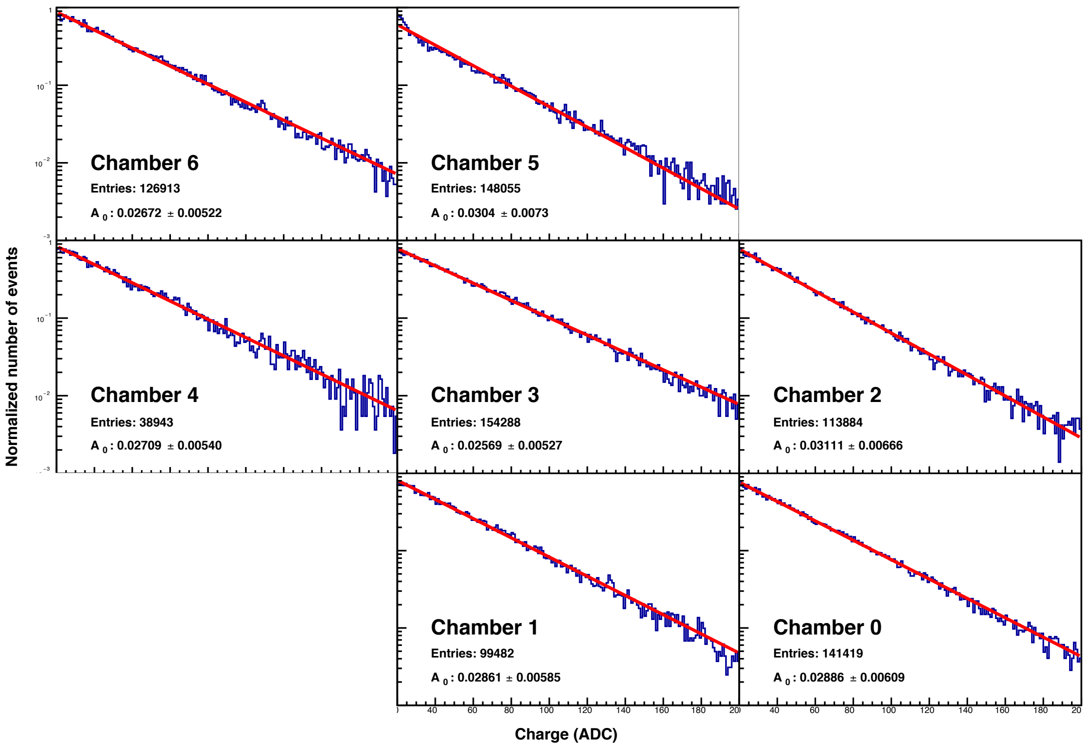

FIG. 5. Charge distribution for Cherenkov photons measured at each RICH chamber. It follows an exponential distribution due to the properties of the Cherenkov counter. For each chamber, the normalization factor A_0 in Equation 6 is calculated.

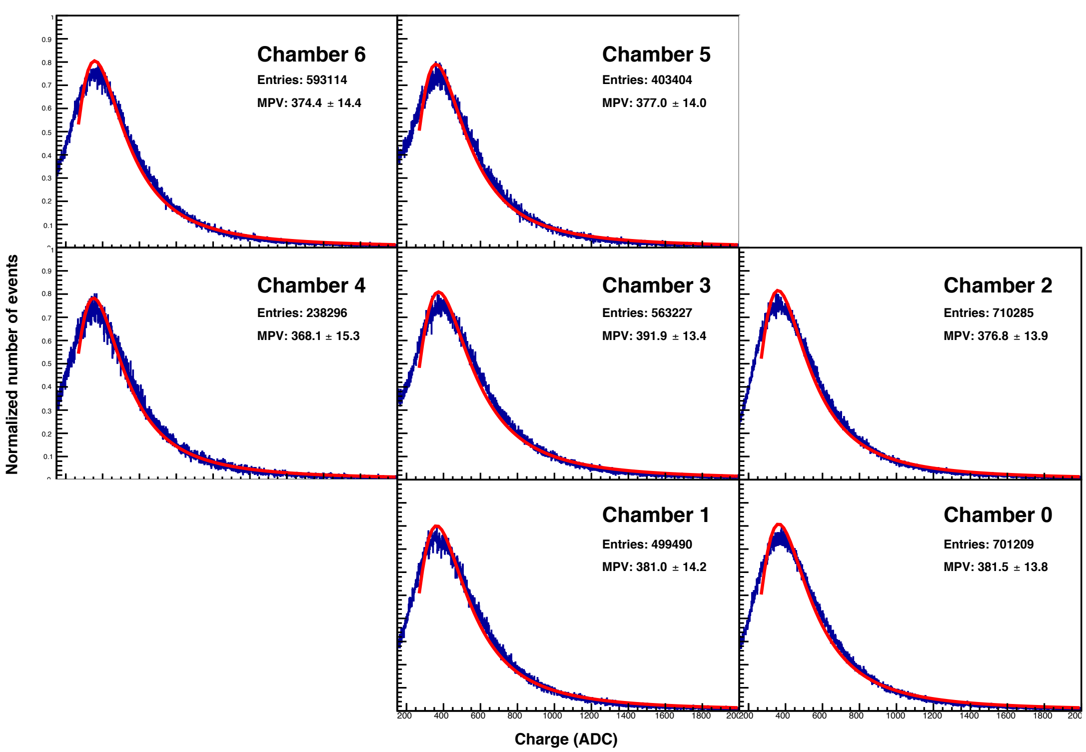

FIG. 6. Charge distribution for minimum ionizing particles measured at each RICH chamber. It follows a Landau distribution due to energy deposition by ionization of surrounding atoms. The most probable value (MPV) is calculated for each chamber.

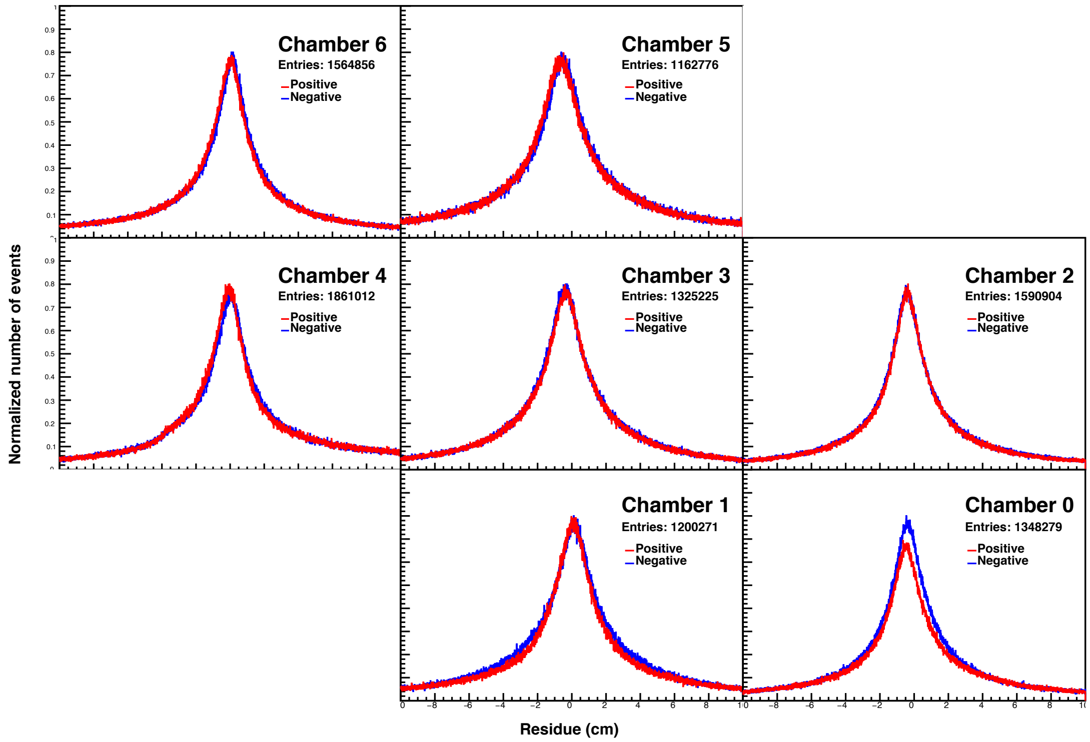

(a)

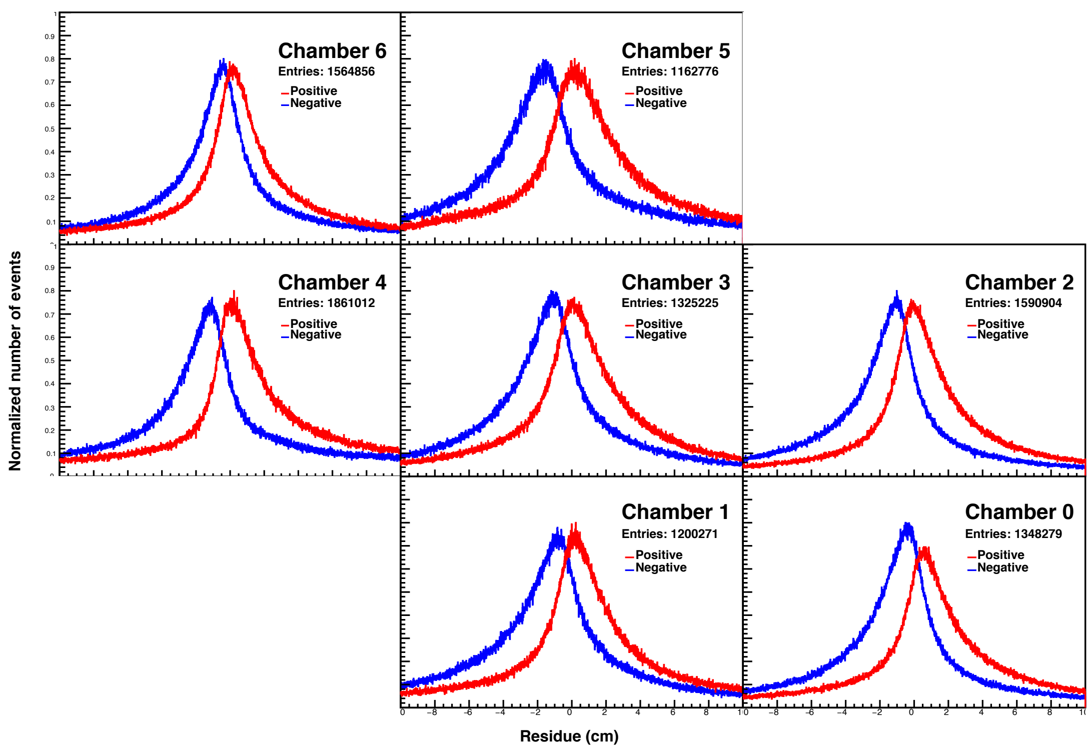

(b)

FIG. 7. Residue distribution for minimum ionizing particles measured at each RICH chamber. Residue is calculated as the cluster position at HMPID subtracted by the extrapolated position from the central tracking system. (a) Residue in the x coordinate, which is the beam direction. (b) Residue in the y coordinate, which is perpendicular to the beam direction on the detector surface.

TABLE I. Proportion of total tracks in each multiplicity class.

Multiplicity	Proportion	Multiplicity	Proportion	Multiplicity	Proportion	Multiplicity	Proportion
$0-5\%$	0.1525	$10-20\%$	0.1913	$40-60\%$	0.1638	$80-100\%$	0.0230
$5-10\%$	0.1177	$20-40\%$	0.2703	$60-80\%$	0.0815		

TABLE II. Proportion of total tracks in each p_T class.

p_T (GeV/c)	Proportion	p_T (GeV/c)	Proportion	p_T (GeV/c)	Proportion	p_T (GeV/c)	Proportion
$1.5-1.6$	0.1299	$2.2-2.3$	0.0478	$2.9-3.0$	0.0178	$4.2-4.4$	0.0073
$1.6-1.7$	0.1135	$2.3-2.4$	0.0414	$3.0-3.2$	0.0289	$4.4-4.6$	0.0060
$1.7-1.8$	0.0981	$2.4-2.5$	0.0359	$3.2-3.4$	0.0224	$4.6-4.8$	0.0048
$1.8-1.9$	0.0850	$2.5-2.6$	0.0308	$3.4-3.6$	0.0176	$4.8-5.0$	0.0040
$1.9-2.0$	0.0736	$2.6-2.7$	0.0268	$3.6-3.8$	0.0139	$5.0-5.5$	0.0074
$2.0-2.1$	0.0635	$2.7-2.8$	0.0234	$3.8-4.0$	0.0112	$5.5-6.0$	0.0047
$2.1-2.2$	0.0551	$2.8-2.9$	0.0205	$4.0-4.2$	0.0088		

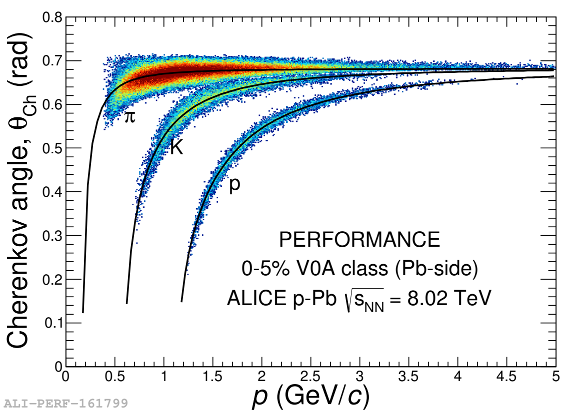

FIG. 8. Cherenkov angle $\theta_{\rm Ch}$ as a function of momentum p. Three bands, corresponding to pions, kaons, and protons, are clearly visible. The lines drawn represent the theoretical p dependence of $\theta_{\rm Ch}$. This figure is extracted from the official ALICE performance report.

In the MWPC, the photoelectron pulse height is known to be distributed as

$$P(A) = \frac{1}{A_0} e^{-A/A_0}, \tag{6}$$

where A is charge and A_0 is a normalization factor [5]. Figure 5 shows the charge distribution of photoelectrons produced by Cherenkov photons, which indeed fits an exponential distribution. Incident MIP create signals in the RICH chambers by depositing energy through the ionization of surrounding atoms. Thus, the cluster charge should follow a Landau distribution, which is indeed the case in Figure 6. In order to characterize tracking effects, it is also important to determine the incident position of MIP on the detector. A residue is calculated for each MIP as the difference between the reconstructed charged-particle cluster position at the HMPID and the track extrapolation from the central tracking system. Figure 7 shows the distribution of this residue for positive and negative charges, where the x coordinate is in the beam direction and the y coordinate is perpendicular to the beam direction on the detector surface. The x residue distribution centers on zero as expected. The y residue distributions shift in opposite directions due to imperfect knowledge about the magnetic field and material budget up to the HMPID chambers.

B. Event and track selection

Several track selection criteria are imposed on the data. To exclude fake cluster-match associations, residue between reconstructed position and track extrapolation is required to be less than 5 cm. To exclude electronic noise, analog-to-digital converted (ADC) charge is required to be greater than 120 ADC. Tracks must also be reconstructed in both the ITS and the TPC. Other additional track selection criteria imposed are based on the number of space points, the quality of track fit, and the distance of closest approach to the reconstructed collision vertex [9]. In order to ensure good detector acceptance and particle identification performance, tracks are selected in the rapidity interval $0 < y < 0.5$.

The data is divided into seven multiplicity classes based on total charge deposited in the V0A detector. For example, the 0-5% multiplicity class contains the 5% of events with greatest multiplicity. The data is also divided into 27 transverse momentum (p_T) classes between 1.5-6.0 GeV/c. Each p_T class contains only the particle tracks that have transverse momentum within its range. The multiplicity and p_T class intervals are detailed in Tables I and II, respectively.

III. RESULTS AND DISCUSSION

In order to understand the multiplicity and p_T dependence of QGP properties, the number of particles pro-

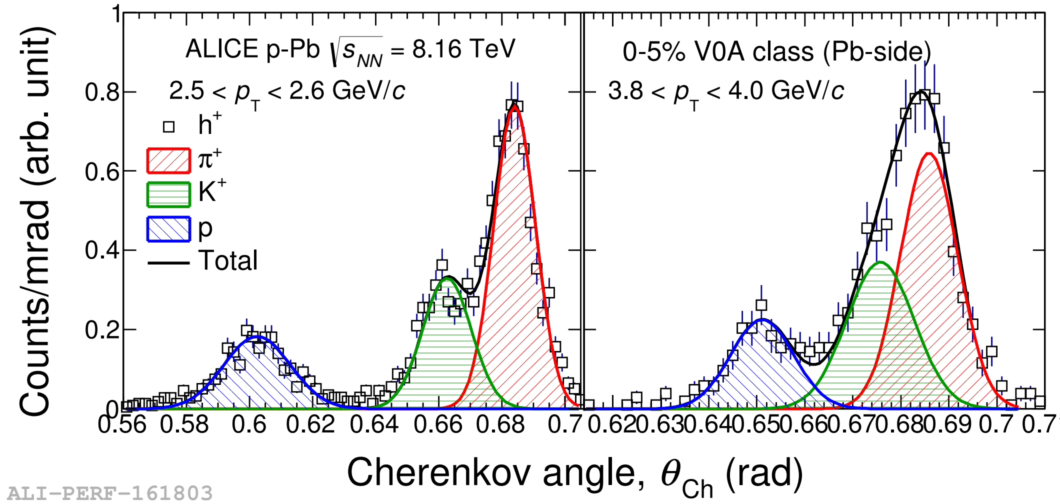

FIG. 9. Example of Gaussian fits for the 2.5-2.6 GeV/c and 3.8-4.0 GeV/c p_T classes of the 0-5% multiplicity class. Each Gaussian corresponds to a particle species, namely pions, kaons, or protons. Particle yield is calculated by taking the integral over Cherenkov angle θ_{Ch} for each Gaussian fit. This figure is extracted from the official ALICE performance report.

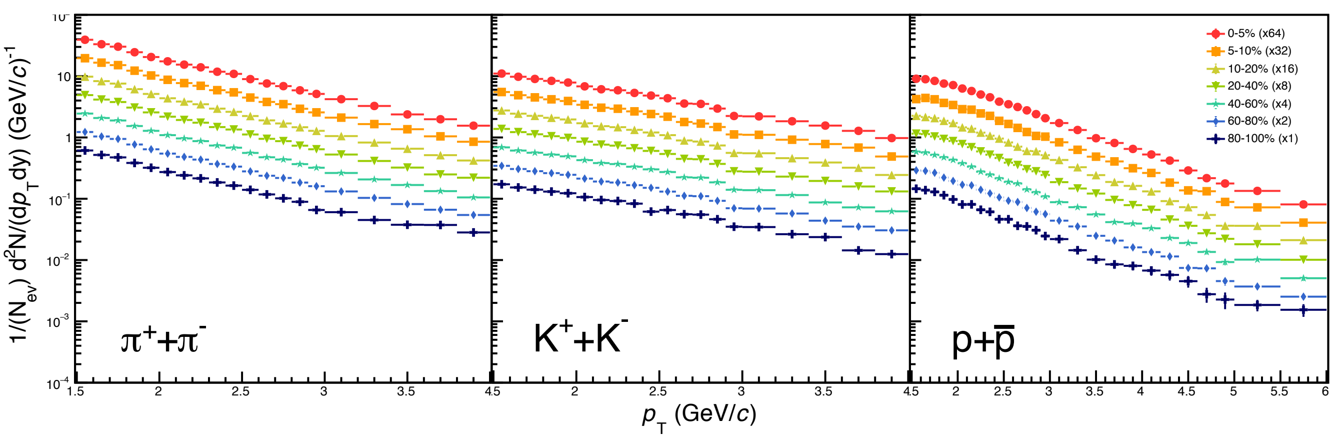

FIG. 10. Detector p_T spectrum (normalized to the number of events) for each particle type measured at the HMPID. There is a strong p_T dependence, where particle yield decreases for higher p_T. Multiplicity classes have been scaled by the indicated factors for better visibility.

duced in each multiplicity and p_T class should be calculated. Particle yield is calculated in three steps. The first step is to create a Cherenkov angle distribution after applying the track selection cuts detailed in Section 3.2. The next step is to integrate over Cherenkov angle and find the number of particles detected. The final step is to correct the detected yield in order to deduce the total yield for each particle species.

A. Cherenkov angle

From the charges measured, Cherenkov photons are selected by the Hough Transform Mehthod (HTM), which discriminates the signal from the background [9]. For each track, the Cherenkov angle θ_{Ch} is calculated as the weighted mean of the individual photon angles. Figure 8 shows θ_{Ch} as a function of track momentum. Three bands are clearly visible in the figure, corresponding to signals from pions, kaons, and protons. The separation is due to their differences in mass, resulting in different speeds and hence θ_{Ch} at the same momentum.

B. Particle yield

Particle identification is performed by statistical unfolding of the Cherenkov angle θ_{Ch}. After applying track

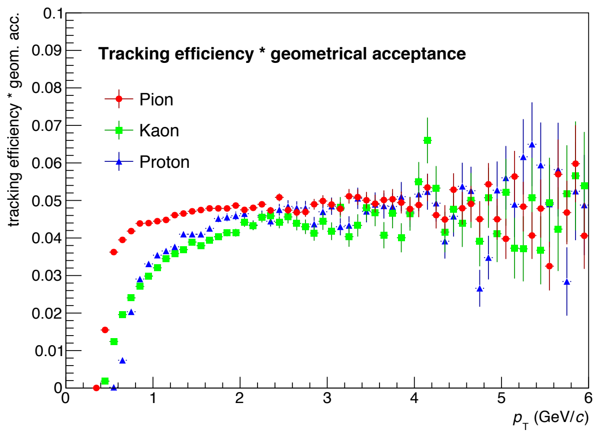

FIG. 11. Tracking efficiency convoluted with geometrical acceptance as a function of p_T. This efficiency rises from ∼4% to ∼6% in the HMPID particle identification p_T range.

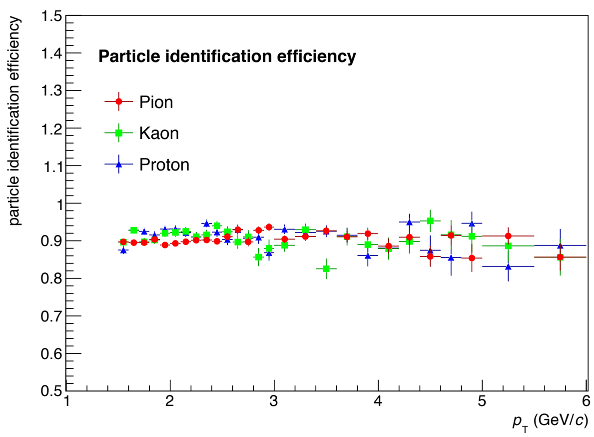

FIG. 12. Particle identification efficiency as a function of p_T. This efficiency is consistently ∼90% across the HMPID particle identification p_T range.

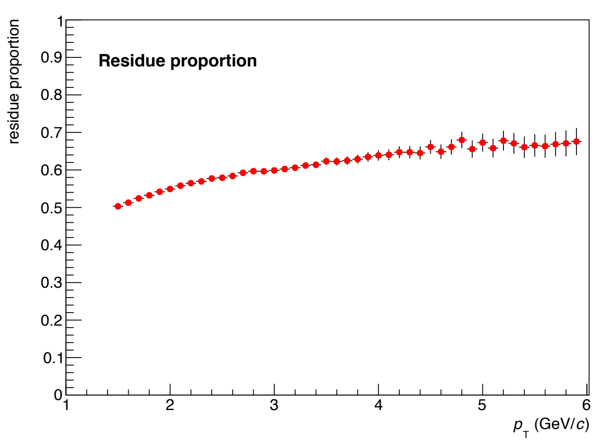

FIG. 13. Proportion of tracks within the 5 cm residue cut as a function of p_T. This efficiency rises from ∼50% to ∼70% in the HMPID particle identification p_T range.

selection cuts, reconstructed Cherenkov angle distributions are created for each multiplicity and p_T class. Each Cherenkov angle distribution is fit using a sum of three Gaussian distributions, corresponding to pions, kaons, and protons. The fit is done by setting initial values of fit parameters to expected values and having yield as a free parameter. Expected value for mean $\langle\theta_{\rm Ch}\rangle$ is calculated from the equation

$$\langle\theta_{\rm Ch}\rangle = \arccos\left(\frac{1}{n\beta}\right) = \arccos\left(\frac{\sqrt{p^2+m^2}}{np}\right) \quad (7)$$

where p is particle momentum and m is particle mass [8]. Expected value for resolution is obtained from Monte-Carlo simulation of the detector response. Parameters are constrained to a mean value of $[\langle\theta_{\rm Ch}\rangle - 2\sigma, \langle\theta_{\rm Ch}\rangle + 2\sigma]$ and a resolution of $[\sigma - 0.1\sigma, \sigma + 0.1\sigma]$. The allowed range is to account for reasonable deviations due to running conditions of the detector. Figure 9 gives examples of Gaussian fits for the reconstructed Cherenkov angle distributions in the 2.5-2.6 GeV/c and 3.8-4.0 GeV/c p_T classes of the 0-5% multiplicity class.

Yield of each particle species is calculated by taking the integral of the corresponding Gaussian distribution. The yield is normalized by dividing the number of events $N_{\rm ev}$ in each multiplicity class. Figure 10 shows the p_T spectrum for each multiplicity class. The result is as expected, with yield decreasing for higher p_T [9].

C. Corrections

The results from Section III B give the number of particles identified in the HMPID. In order to deduce the total number of particles produced during collision, several corrections need to be implemented. This includes adjusting for HMPID tracking efficiency and geometrical acceptance, particle identification efficiency, and track selection cuts. Some additional corrections remain but have only small effects.

Tracking efficiency and geometrical acceptance is obtained from Monte-Carlo simulation. In Monte-Carlo simulation, the total number of particles produced is known and the detector signal can be simulated. The ratio between detected particles and total particles is fit with a polynomial function, as is shown in Figure 11. This function is then applied to the particle yield from Section III B to correct for tracking efficiency and geometrical acceptance. For each particle species, the tracking efficiency convoluted with geometrical acceptance increases from ∼4% at 1.5 GeV/c to ∼6% at higher p_T. The small efficiencies at low p_T is because the particle velocities are below the Cherenkov effect threshold, and Cherenkov photon are not yet produced.

Particle identification efficiency is obtained by applying a similar analysis as Section III B to Monte-Carlo simulated data. In Monte-Carlo data, each particle species is known. Thus, the Cherenkov distributions can be created

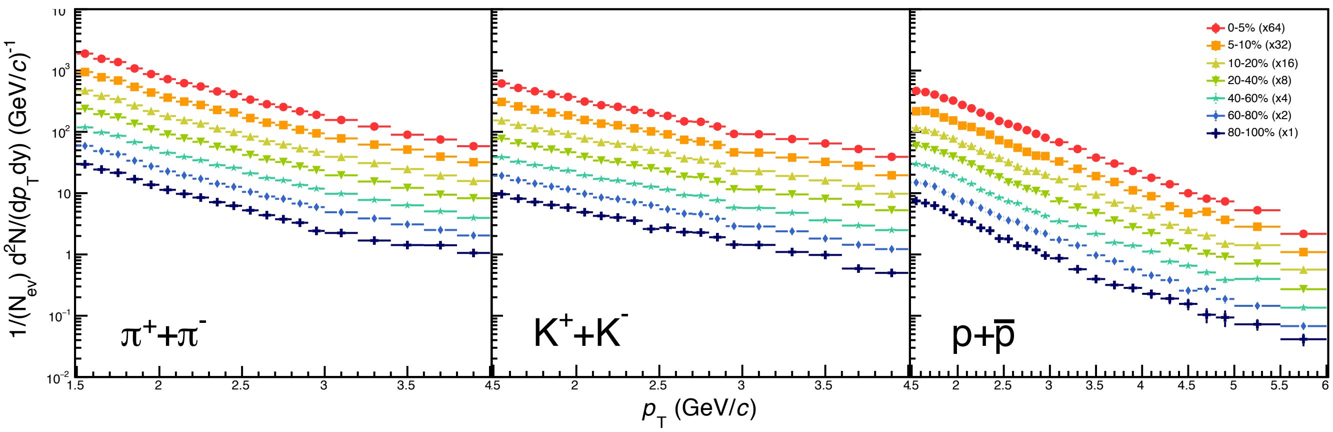

FIG. 14. Total p_T spectrum (normalized to the number of events) after corrections for efficiencies and track selection cuts. There remains a strong p_T dependence, where particle yield decreases at higher p_T. Each multiplicity class has been scaled by the indicated factors for better visibility.

separately for each particle species. These Cherenkov distributions are fit in the same way as Section III B and the simulated number of identified particles can be calculated. The particle identification efficiency is then the ratio between identified particles and total particles produced, and is shown in Figure 12. A linear fit is calculated for the ratio and is applied to correct the particle yield for particle identification efficiency. The particle identification efficiency reaches ∼90% and is consistent across p_T values.

Corrections for track selection cuts come mainly from the residue cut of 5 cm. Real data is used to calculate the ratio between candidate tracks that pass the residue cut and all candidate tracks within the detector acceptance. A polynomial fit is calculated for this ratio, as shown in Figure 13, and is applied to correct the particle yield for residue cuts. This ratio increases from ∼50% at 1.5 GeV/c to ∼70% at higher p_T.

Applying corrections to the detector yield obtained in Section III B gives the total particle yield. Figure 14 shows the p_T spectrum for the total number of particles produced in the LHC16r sample. After the corrections, the particle yield maintains a strong p_T dependence, where yield decreases for higher p_T. This can be explained because hard particle production is less probable than soft particle production during hadronization. When comparing multiplicity classes, there is a slight hardening of the spectra for higher multiplicities. This effect is stronger in protons than in pions and kaons.

IV. CONCLUSION

In this report, we analyzed data from p-Pb collisions at $\sqrt{s_{\mathrm{NN}}} = 8.16$ TeV in 2016 during LHC Run 2. Performance of the HMPID detector was characterized in terms of the Cherenkov photon charge distribution, MIP charge distribution, and residue distributions. The HMPID measurements were found to agree with expected results, thus validating the HMPID data. Particle identification was done by statistical unfolding of the Cherenkov angle, and total particle yield was deduced after applying several corrections. Particle yield shows a strong dependence on track momentum, where yield decreases for higher p_T, and a very slight dependence on multiplicity, where the spectra hardens for higher multiplicities.

The results from HMPID can be combined with analysis from ITS, TOF, and TPC to identify pions, kaons, and protons up to 20 GeV/c in the p_T spectrum [9]. The particle yield can then be used to do comparative studies with proton-proton (pp) and lead-lead (Pb-Pb) collisions. Since QGP is supposed to form in Pb-Pb collisions and not in p-Pb collisions, its properties can be studied by examining the differences between these two collision modes. One such measurement is the nuclear modification factor, which is a ratio between the particle yield and the pp collision cross section normalized to the number of binary collisions. The nuclear modification factor is suppressed at high p_T for Pb-Pb collisions but not for p-Pb collisions [10], which is strong evidence for jet quenching and the formation of QGP.

ACKNOWLEDGMENTS

I would like to thank my supervisor, Giacomo Volpe, for his guidance during my studentship. I am also grateful to CERN and its relevant members for their support of the student program. Finally, I would like to thank the HKUST School of Science and Department of Physics for providing this wonderful opportunity.

[1] C. Lippmann, Particle identification in alice boosts qgp studies, https://cerncourier.com/a/particle-identification-in-alice-boosts-qgp-studies/ (2012), cERN Courier.

[2] ALICE Collaboration, ALICE, http://alice.web.cern.ch/ (retrieved 2019), online.

[3] CERN, Heavy ions and quark-gluon plasma, https://home.cern/science/physics/heavy-ions-and-quark-gluon-plasma (retrieved 2019), online.

[4] B. Alessandro *et al.*, *ALICE: Physics Performance Report. ALICE physics performance : Technical Design Report*, Technical Design Report ALICE, Vol. 32 (CERN, Geneva, 2005) revised version submitted on 2006-05-29 15:15:40.

[5] F. Piuz, W. Klempt, L. Leistam, J. De Groot, and J. Schkraft (ALICE Collaboration), *ALICE high-momentum particle identification: Technical Design Report*, Technical Design Report ALICE (CERN, Geneva, 1998).

[6] G. Volpe (ALICE Collaboration), The high momentum particle identification (hmpid) detector pid performance and its contribution to the alice physics program, Nuclear Instruments and Methods in Physics Research Section A: Accelerators, Spectrometers, Detectors and Associated Equipment **876**, 133 (2017), the 9th international workshop on Ring Imaging Cherenkov Detectors (RICH2016).

[7] ALICE Collaboration, More details on the alice hmpid, http://alice.web.cern.ch/detectors/more-details-alice-hmpid (retrieved 2019), online.

[8] E. Nappi and J. Seguinot, Ring imaging cherenkov detectors: The state of the art and perspectives, in *La Rivista del Nuovo Cimento*, Vol. 28 (Italian Physical Society, Bologna, 2005) pp. 1–130.

[9] J. Adam *et al.* (ALICE Collaboration), Multiplicity dependence of charged pion, kaon, and (anti)proton production at large transverse momentum in ppb collisions at $\sqrt{s_{NN}} = 5.02$ tev, Physics Letters B **760**, 720 (2016).

[10] J. Adam *et al.* (ALICE Collaboration), Centrality dependence of the nuclear modification factor of charged pions, kaons, and protons in pb-pb collisions at $\sqrt{s_{NN}} = 2.76$ tev, Physics Review C **93**, 034913 (2016).